TRANSCENDING THE PORE STRUCTURE OF A CEMENT PASTE: A 3D EFFECTIVE MEDIA LATTICE BOLTZMANN APPROACH

M. Zalzale (1), P.J. McDonald (2) and K.L. Scrivener (1)

(1) Laboratory of Construction Materials, Ecole Polytechnique Fédérale de Lausanne, 1015 Lausanne, Switzerland

(2) Department of Physics, University of Surrey, Guildford, Surrey, GU2 7XH, UK

mohamad.zalzale@epfl.ch

Abstract

A three-dimensional lattice Boltzmann model based on the effective media approach is used to calculate the intrinsic permeability of cement microstructures determined using the model μIC. The model comprises capillary pores, C-S-H gel pores and solid phases. The C-S-H phase is assigned a very low permeability and does consequently connect the depercolated capillary pores and air voids.

It is found that when the modelled capillary porosity corresponds to the volume of water-accessible capillary pores and air voids, as measured by ^{1}H nuclear magnetic resonance relaxation analysis, the modelled permeability is in very good agreement with water permeability experiments.

Key Words: Cement; Permeability; Lattice Boltzmann; Effective Media

1. INTRODUCTION

It is of great economical and ecological interest to design new concretes with improved and predictable resistance to degradation. Water is involved in almost every form of deterioration and techniques for assessing the durability of cementitious materials include porosity and permeability tests. Cement paste is the continuous porous matrix that binds the aggregates to form concrete and has consequently a considerable influence on its permeability. The permeability of cement paste is difficult to measure and reported values vary widely. Table I shows measured permeability values for cement pastes with a water-to-cement ratio of approximately 0.40.

Table I: Experimental permeability values for mature cement paste with a water-to-cement ratio (*w/c*) of approximately 0.40

	Method	*w/c*	Hydration age (days)	Intrinsic permeability (m^2)
Nyame & Illston 1981 [1]	Standard permeability cell	0.47	600	5×10^{-22}
Banthia and Mindess 1989 [2]	Tri-axial permeability cell	0.35	28	8.9×10^{-20}
Ai *et al.* 2001 [3]	Thermopermeametry [4]	0.40	548	10^{-22}
Vichit-Vadakan & Scherer 2002 [5]	Beam-bending [6]	0.40	14	5×10^{-22}
Vichit-Vadakan & Scherer 2003 [7]	Beam-bending [6]	0.45	3	6×10^{-22}
Ye 2005 [8]	Three parallel permeability cells	0.40	28	9×10^{-21}
Grasley & Scherer 2007 [9]	Dynamic pressurization [10]	0.40	14	2×10^{-21}

The intrinsic permeability characterises a porous medium from the perspective of saturated flow through it. Intrinsic permeability depends on the pore network and is theoretically independent of the penetrating fluid. It is related to macroscopic observables through Darcy's law [11] as $\kappa = \frac{L}{A}\frac{Q\mu}{\Delta P}$ where κ is the intrinsic permeability of a sample of length L and cross-sectional area A through which a fluid flow Q is driven by an applied pressure gradient ΔP. The dynamic fluid viscosity μ is the product of the density ρ by the kinematic viscosity υ. The intrinsic permeability κ is expressed in units of m^2.

The scatter in the data shown in table I is considerable even when comparing the permeability of samples with similar water-to-cement ratios (*w/c*) and hydration ages. For instance, at the age of 28 days, the permeability of the *w/c*=0.35 sample of Banthia and Mindess [2] is 10 times higher than the permeability of the *w/c*=0.40 sample of Ye et al. [8]. In addition to the differences in the experimental setups and samples preparation, this

discrepancy can be attributed to (1) the use of cyclic flow reversals by Banthia and Mindess that may have led to the expulsion of pore-blocking micro-particles and (2) the fact that the samples of Banthia and Mindess were sealed for 24 hours and then cured underwater for 27 days while the samples of Ye *et al.* [8] were sealed for 28 days and then vacuum saturated just before the experiment suggesting that the samples of Banthia and Mindess were more saturated (had less air voids). Furthermore, in experiments where the cement composition, sample preparation, *w/c* and hydration age [5, 9] are the same, the discrepancy may be as large as half an order of magnitude (5×10^{-22} [5] and 2×10^{-21} m^2 [9]). Besides the differences in the experimental setups, this deviation can be attributed to the different sealing times: for water-cured samples, the shorter sealing time (before water curing) may lead to a higher degree of saturation, to less air voids and thus to higher water permeability.

Permeability experiments are time-consuming and subject to a big variability. Numerical models provide a promising alternative. They rely on the simulation of the flow inside the pore structure of the cement paste. The pore structure can be extracted from micro-tomographs or from microstructural models of cement hydration such as HYMOSTRUC [12], CEMHYD3D [13] and μIC [14]. Afterwards, the Navier-Stokes equation is numerically solved inside this pore network. Lattice Boltzmann (LB) methods are a class of computational fluid dynamics solvers [15] that can be used to solve the flow. In general, the LB methods are employed because they (1) are easier to implement than conventional finite element methods, (2) deal implicitly with arbitrarily shaped geometries and (3) are readily parallelizable making efficient use of modern day central processing and graphics processing units.

Garboczi and Bentz [16] used a lattice Boltzmann model to calculate the permeability of CEMHYD3D cement microstructures as a function of capillary porosity and microstructure resolution. They reported that the calculated permeability was very sensitive to the resolution of the microstructure and at the highest resolution studied (0.25 μm), the permeability was circa 10^{-17} m^2 at a capillary porosity of 12%. We previously [17] used the LB method to calculate the permeability of μIC cement microstructures for different *w/c* ratios, degrees of hydration, microstructure and LB resolutions. We reported a permeability of 1.6×10^{-18} m^2 for *w/c*=0.40, hydration age of 283 days and a microstructure resolution of 1 μm. Scaling tests showed that this permeability would decrease by more than one order of magnitude when the resolutions of the microstructure and of the LB solvers are increased. Additionally, we had extended the model to study the adsorption and desorption of liquid and vapour as a two-phase fluid in the same model μIC microstructures. Most recently, Zhang *et al.* [18] used the LB method to calculate the permeability of HYMOSTRUC cement microstructures. They reported a permeability of approximately 2×10^{-18} m^2 for *w/c*=0.40, hydration age of 50 days and a microstructure resolution of 0.5 μm.

In the above lattice Boltzmann applications to cement, the water permeability is overestimated by several orders of magnitude. At the core of this problem is that the conventional LB method can handle only two types of nodes: (1) pores with free fluid flow and (2) solids where the no-slip boundary condition is usually applied. This is inconvenient for multi-scale heterogeneous porous media because resolving the flow requires an excessive amount of computational resources. Traditional approaches for tackling multi-scale problems with the LB method include the use of multi-scale grids [19] and memory-efficient

implementations [20] but their application remains limited because they are difficult to implement. Furthermore, the use of these multi-scale approaches is not very promising for cement because the 3D nanostructure of the C-S-H gel is still an area of active debate. Recent ^{1}H nuclear magnetic resonance relaxation analysis by Muller *et al.* [21] revealed that the water-filled capillary porosity in undried mature cement paste can be as low as 1%. This suggests that at high degrees of hydration, the water-filled capillary pore network is depercolated and the permeability is controlled by the smaller C-S-H gel pores. Hence, the simulations do overestimate the permeability because they are applied inside a percolated capillary pore network which does not capture the complexity of the actual cement pore structure [22].

A distinctive class LB methods is based on the effective media approach and has the potential to bridge the gap between the nano- and macroscopic scales. In the effective media approach, the multi-scale problem is addressed by assigning effective macro-scale properties (*i.e.* permeability) to some nodes (partially permeable pores) and is capable of extending the use of the standard LB method to include larger media or media with partly unknown geometry. Nonetheless, the application of such methods has been limited so far to one or more of the following: (1) two dimensions, (2) percolated media, (3) media with only two phases (*e.g.* pores and partially permeable pores, no solids) or (4) were unstable at low permeabilities.

In this paper, we use a 3D LB model based on the effective media approach to calculate the permeability of cement model microstructures determined using the model μIC. The model comprises capillary pores, C-S-H gel pores and solid phases. The bulk C-S-H is assigned a very low permeability and does consequently act as a low permeability phase that connects the depercolated water-filled capillary pores and air voids. The intrinsic permeability is studied as a function of the volume of capillary porosity.

2. LATTICE BOLTZMANN METHOD

2.1 Mathematical description of the lattice Boltzmann method

In this section, we provide a brief mathematical outline of a three-dimensional partial bounce-back algorithm as initially developed in two dimensions by Walsh *et al.* [23]. In the LB method, the fluid is represented by a density distribution of Q fluid elements each with a defined lattice velocity performing consecutive propagation and collision steps over a discrete lattice mesh. Under appropriate conditions (*i.e.* collision matrix, relaxation parameters, equilibrium functions and lattice parameters), the basic equation can be encapsulated in:

$$f_i\left(\boldsymbol{r}+\boldsymbol{e}_i,t+1\right)=f_j^{eq}\left(\boldsymbol{r},t\right)=\omega_i\rho^*\left(1+3\boldsymbol{u}^*.\boldsymbol{e}_i+\frac{9}{2}\left(\boldsymbol{u}^*.\boldsymbol{e}_i\right)^2-\frac{3}{2}\boldsymbol{u}^*.\boldsymbol{u}^*\right) \quad (1)$$

The functions f_i represent the density of particles moving at position $\boldsymbol{r}$ with velocity $\boldsymbol{e}_i$ and at time t. The equilibrium distribution $f_j^{eq}\left(\boldsymbol{r},t\right)$ encapsulates the physics of the problem (e.g. Navier-Stokes) and the coefficients ω_i are lattice weights specific to the chosen lattice. The equilibrium moments ρ^* and $\rho^*\boldsymbol{u}^*$ are equal to the macroscopic density and momentum

which are calculated from the distribution functions as $\rho(\boldsymbol{r},t)=\sum_{i=1}^{Q} f_i(\boldsymbol{r},t)$ and $\rho(\boldsymbol{r},t)\boldsymbol{u}(\boldsymbol{r},t)=\sum_{i=1}^{Q} f_i(\boldsymbol{r},t)\boldsymbol{e}_i$, respectively. Under these conditions, the fluid kinematic viscosity is $\upsilon=1/6$.

For the fluid-solid collision, the no-slip boundary condition [24] is used: if a fluid element hits a solid boundary following the propagation step, its momentum is reversed with:

$$f_i(\boldsymbol{r}+\boldsymbol{e}_i,t+1)=f_{\tilde{i}}(\boldsymbol{r},t) \tag{2}$$

where $\tilde{i}$ is the direction opposite to i: $\boldsymbol{e}_i=-\boldsymbol{e}_{\tilde{i}}$.

To account for the partial bounce-back step, the effective media parameter $\sigma(\boldsymbol{r})$ is introduced. The streaming, fluid-fluid and fluid-solid collision steps are combined in:

$$f_i(\boldsymbol{r}+\boldsymbol{e}_i,t+1)=(1-\sigma(\boldsymbol{r}))\,f_j^{eq}(\boldsymbol{r},t)+\sigma(\boldsymbol{r})\,f_{\tilde{i}}(\boldsymbol{r},t). \tag{3}$$

The microscopic moments are unchanged and the macroscopic moments become:

$$\rho(\boldsymbol{r},t)=(1-\sigma(\boldsymbol{r}))\sum_{i=1}^{Q} f_i(\boldsymbol{r},t) \tag{4}$$

$$\rho(\boldsymbol{r},t)\boldsymbol{u}(\boldsymbol{r},t)=(1-\sigma(\boldsymbol{r}))\sum_{i=1}^{Q} f_i(\boldsymbol{r},t)\boldsymbol{e}_i \tag{5}$$

2.2 Implementation and validation of the algorithm

The simulations are performed on a three-dimensional cubic lattice with 19 velocities (D3Q19). Pressure boundary conditions are implemented as described by Narváez and Harting [25]. For the two other spatial directions periodic boundary conditions are used to minimize boundary effects. We considered the simulation converged when the mean velocity change per voxel per time step averaged over 1000 time steps was less than one part in a million. Afterwards, the pressure gradient was calculated as described by Narváez *et al.* [26] and the permeability using Darcy's law.

To verify that the model recovers the standard lattice Boltzmann model behaviour, we compared numerical and theoretical permeabilities, as defined by Darcy's law, for a flow between two parallel plates with a constant cross section [27]. The relative error in permeability $\varepsilon(\kappa)=\left|\kappa^{LB}-\kappa^{theory}\right|/\kappa^{theory}$ decreases from 13 to 1% when the channel width increases from 3 to 7 nodes. To test the accuracy of the model in a more complicated geometry, we computed the flow past a cubic array of overlapping spheres [28]. We varied the box size while keeping the porosity at circa 20%. The relative error in permeability decreases from 3.8 to 1% when the box size increases from 21 to 71 lattice node.

To validate the partial bounce-back model, we computed the permeability of a sample filled with nodes with an effective media parameter $\sigma(\boldsymbol{r})=\sigma\ \forall\boldsymbol{r}$. Walsh *et al.* [23] derived the permeability of such media as a function of σ and the fluid kinematic viscosity υ:

$$\kappa=\frac{1-\sigma}{2\sigma}\upsilon. \tag{6}$$

Figure 1 shows the calculated and analytical permeabilities as a function of the effective media parameter σ. The error is negligible for homogeneous media with permeability $\kappa > 10^{-2}\Delta x^2$, less than 1% for $\kappa \geq 10^{-6}\Delta x^2$ and less than 7.5% for $\kappa < 10^{-6}\Delta x^2$. For cement paste, Δx is on the order of 10^{-6} to 10^{-7} m^2.

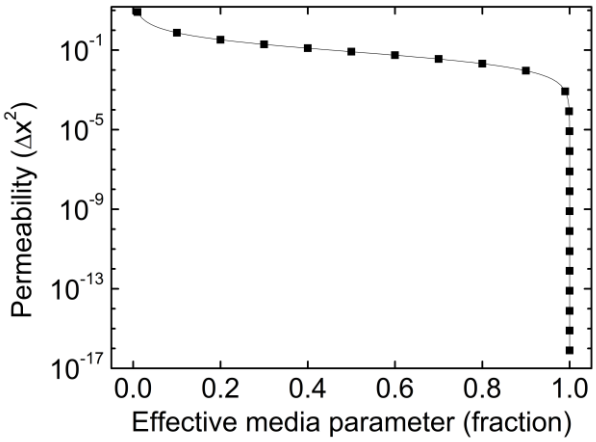

Figure 1: Analytical (solid line) and LB simulated (squares) permeabilities of a homogeneous system as a function of the effective media parameter σ. The analytical values are calculated with equation (6)

We note that for homogeneous media, the number of spatial dimensions does not matter so that the results reported above are in excellent agreement with the two-dimensional simulations performed by Walsh *et al.* [23]. It should be pointed out that the effective media parameter σ should not be used to calculate the porosity $\phi = 1 - \sigma$ of the system. Alternatively, σ should be regarded as an internal model parameter from which the permeability is derived with the help of equation (6) [23]. Additionally, we verified that mass is conserved up to numerical accuracy in homogeneous and heterogeneous media and that the pressure drop in homogeneous media is linear inside the sample.

3 APPLICATION TO CEMENTITIOUS MATERIALS

3.1 Cement model microstructures

We obtained cement model microstructures using the vector model μIC [14] with a water-to-cement (*w/c*) ratio of 0.40. The model cement clinker is similar to a U.S. type III cement and the reaction kinetics were defined according to the hydration model of Parrot and Killoh [29]. The reactant and hydrate (except C-S-H) densities were set to standard literature values. Recently, the density of C-S-H was found to be time-dependent in ^{1}H nuclear magnetic resonance relaxation analysis by Muller *et al.* [21]. For example, at 28 days the bulk density of C-S-H is $\rho_{C-S-H} = 1.96$ g/cm^3. The time-dependent densities can be found in ref. [21] and are in very good agreement with the findings of Do *et al.* [22].

In terms of capillary pore structure, Muller *et al.* [21] recently showed by ^{1}H nuclear magnetic resonance relaxation analysis that for a white cement paste with *w/c*=0.40 after 28

days of hydration, the volume of remaining capillary water is 1.4%. For the same sample, the volume of the chemical shrinkage voids is 7.8%. The volume of the accessible capillary pore network (water-filled capillary pores and air voids) must be bound between the volume of water-filled capillary pores (lower bound) and the volume of water-filled capillary pores and air voids (upper bound: 9.2%). Since the microstructure modelling platforms implicitly combine the capillary pores and the chemical shrinkage voids, we take as input a hydrated microstructure where the total capillary porosity equates to the experimentally measured water-filled capillary pores and air voids. We start with a microstructure with 9.2% capillary porosity obtained at a degree of hydration of 89%. Next, using a modified version of the intrusion porosimetry algorithm developed by Do *et al.* [22], we transformed a fraction of the largest pores into air voids by making them inaccessible to transport. By doing so, we can study the permeability of the paste as a function of the water-filled capillary porosity and air voids.

With regard to the C-S-H gel porosity, Powers showed that the coefficient of permeability of the gel itself is about 7×10^{-23} m^2 [30]. We ascribe this permeability to all the C-S-H nodes with the help of equation (6).

Except when stated otherwise, structures generated with the vector model μIC were translated onto a cubic grid with a lattice spacing of 0.5 μm by taking the phase present at the voxel centre as representative of the voxel and simulation volumes comprised 200^3 voxels. The algorithm is run until convergence as defined in section 4. The μIC microstructures were previously tested and found to be isotropic with a permeability normalized standard deviation smaller than 2% [17]. All solid phases excluding C-S-H (*e.g.* alite, portlandite) were treated as impermeable solids with no inherent porosity.

3.2 Permeability of cement model microstructures

Figure 2(a) shows the cement paste permeability as a function of the capillary porosity as described in the previous section. To be in the range of the experimental water permeability (figure 2(b): 10^{-22} to 10^{-19} m^2), the volume of the accessible capillary pore network must be below 5%. In the experiment of Ye [8], the samples were sealed cured for 28 days and then vacuum saturated with water during 4 to 8 hours before the permeability measurement. Muller [31] recently used ^1H nuclear magnetic resonance relaxation analysis to measure the increase of capillary water volume in a sample that was vacuum saturated during 24 hours following 28 days of sealed curing. He reported that he succeeded to fill approximately half of the air voids so that the water-filled capillary porosity increased from 1.38 to 5.5%. Since the samples of Ye were vacuum saturated for a shorter time, the accessible pore space should be smaller than 5.5%. To match the experimental permeability of Ye [8], the accessible capillary porosity in the modelled microstructure should be between 4.2 and 4.0%, a value close to the expected volume of accessible capillary in his samples.

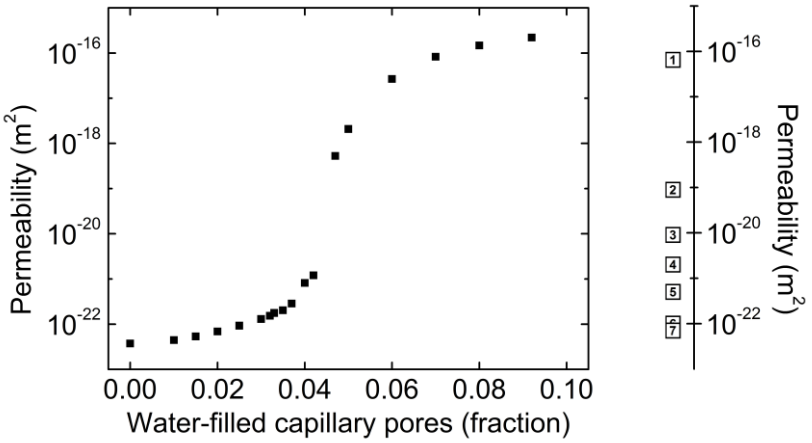

(a) (b)

Figure 2: (a) Simulated permeabilities as a function of the volume of the accessible capillary pore network (water-filled capillary pores and accessible air voids) and (b) experimental permeabilities from top to bottom: (1) Wong *et al.* [32], (2) Banthia & Mindess [2], (3) Ye [8], (4) Grasley & Scherer [9], (5) Nyame & Illston [1], (5) Vichit-Vadakan & Scherer [5, 7], (6) Ai *et al.* [3] and (7) Powers [30]

Elam *et al.* [33] previously reported depercolation of the void regions between mono-sized overlapping randomly located spheres at 3.2% void. We observe a very sharp drop in permeability circa 4% accessible capillary porosity. At the discretisation resolution of 0.5 μm that we used, the depercolation threshold is expected to occur at a higher capillary porosity. The similarities between our results and the theoretical calculations of Elam *et al.* [33] suggest that the introduction of the permeable C-S-H phase to the LB model reduced the effect of the discretisation resolution on the permeability. In a standard discrete model incorporating pores and solids only, a coarse discretisation of two pores that are connected with a very narrow channel and are surrounded by C-S-H can lead to the false conclusion that the two pores are disconnected. By ascribing effective media properties to the C-S-H, the two pores remain connected and the discretisation error decreases.

Below the *effective threshold* of capillary depercolation, the cement permeability strongly depends on the C-S-H permeability and on how the remaining water-filled capillary pores and solid phases play off each other. In this study the permeability of C-S-H was not varied because of the lack of experimental data.

4 CONCLUSIONS

The 3D effective media lattice Boltzmann approach is capable of modelling the flow simultaneously in open regions where the flow is described by the Navier-Stokes equation inside a defined geometry and in porous solids where the flow is described by Darcy's law inside an unknown geometry.

Most cement permeability simulations have been limited to the capillary pore network of the paste. Solving the Navier-Stokes equation in this coarse percolated network leads to an overestimation of the permeability. By making the C-S-H permeable, it is possible to

decrease the capillary porosity to match recent experimental measurements. Furthermore, the presence of the C-S-H reduces the effect of the resolution on the simulated permeability.

It is found that when the modelled capillary porosity corresponds to the volume of water-accessible capillary pores and air voids, as measured by ^{1}H nuclear magnetic resonance relaxation analysis, the modelled permeability is in good agreement with water permeability experiments. The large drop in permeability around 4% accessible capillary porosity could explain a part of the scatter in permeability measurements.

There are no restrictions on the number of permeable phases in the effective media LB model so it can be readily used to bridge the gap between different hierarchical scales. For instance, simulations at the cement paste microscopic scale (capillary pores, C-S-H and solid phases) could be used as input for simulations at the mortar macroscopic scale (cement paste, sand, interfacial transition zones and microcracks) which, in turn, can be used as input for simulations at the concrete macroscopic scale (mortar, aggregates, interfacial transition zones and cracks). The effective media LB model is also readily applicable to porous media such as rocks and fractured media.

ACKNOWLEDGEMENTS

Funding was provided by the European Union (FP7 / 2007-2013, grant 264448), the UK EPSRC (grant number: EP/H033343/1) and Nanocem (www.nanocem.org).

REFERENCES

[1] B.K. Nyame and J.M. Illston, Relationships between permeability and pore structure of hardened cement paste, *Mag. Concrete Res.* **33** (1981) 139-146.

[2] N. Banthia and S. Mindess, Water permeability of cement paste, *Cem. Conc. Res.* **19** (1989) 727-736.

[3] H. Ai, J.F. Young and G.W. Scherer, Thermal Expansion Kinetics: Method to Measure Permeability of Cementitious Materials: II, Application to Hardened Cement Pastes, *J. Am. Ceram. Soc.* **84** (2001) 385-391.

[4] G.W. Scherer, Thermal Expansion Kinetics: Method to Measure Permeability of Cementitious Materials: I, Theory, *J. Am. Ceram. Soc.* **83** (2000) 2753-2761.

[5] W. Vichit-Vadakan and G.W. Scherer, Measuring Permeability of Rigid Materials by a Beam-Bending Method: III, Cement Paste, *J. Am. Ceram. Soc.* **85** (2002) 1537-1544.

[6] G.W. Scherer, Measuring Permeability of Rigid Materials by a Beam-Bending Method: I, Theory, *J. Am. Ceram. Soc.* **83** (2000) 2231-2239.

[7] W. Vichit-Vadakan and G.W. Scherer, Measuring permeability and stress relaxation of young cement paste by beam bending, *Cem. Conc. Res.* **33** (2003) 1925-1932.

[8] G. Ye, Percolation of capillary pores in hardening cement pastes, *Cem. Conc. Res.* **35** (2005) 167-176.

[9] Z.C. Grasley, G.W. Scherer, D.A. Lange and J.J. Valenza, Dynamic pressurization method for measuring permeability and modulus: II. cementitious materials, *Mater. Struct.* **40** (2007) 711-721.

[10] G. Scherer, Dynamic pressurization method for measuring permeability and modulus: I. theory, *Mater. Struct.* **39** (2006) 1041-1057.

[11] H. Darcy, *Les Fontaines Publiques de la Ville de Dijon*, Dalmont, Paris, 1856.

[12] K. van Breugel, Numerical simulation of hydration and microstructural development in hardening cement-based materials (I) theory, *Cem. Conc. Res.* **25** (1995) 319-331.

[13] D.P. Bentz, Three-Dimensional Computer Simulation of Portland Cement Hydration and Microstructure Development, *J. Am. Ceram. Soc.* **80** (1997) 3-21.
[14] S. Bishnoi and K.L. Scrivener, μic: A new platform for modelling the hydration of cements, *Cem. Conc. Res.* **39** (2009) 266-274.
[15] D. Raabe, Overview of the lattice Boltzmann method for nano- and microscale fluid dynamics in materials science and engineering, *Model. Simul. Mater. Sc. Eng.* **12** (2004) 13-46.
[16] E.J. Garboczi and D.P. Bentz, The effect of statistical fluctuation, finite size error, and digital resolution on the phase percolation and transport properties of the NIST cement hydration model, *Cem. Conc. Res.* **31** (2001) 1501-1514.
[17] M. Zalzale and P.J. McDonald, Lattice Boltzmann simulations of the permeability and capillary adsorption of cement model microstructures, *Cem. Conc. Res.* **42** (2012) 1601-1610.
[18] M. Zhang, G. Ye and K.v. Breugel, Microstructure-based modeling of permeability of cementitious materials using multiple-relaxation-time lattice Boltzmann method, *Comp. Mater. Sci.* **68** (2013) 142-151.
[19] J. Tölke, S. Freudiger and M. Krafczyk, An adaptive scheme using hierarchical grids for lattice Boltzmann multi-phase flow simulations, *Comput. Fluids* **35** (2006) 820-830.
[20] C. Pan, J.F. Prins and C.T. Miller, A high-performance lattice Boltzmann implementation to model flow in porous media, *Comput. Phys. Commun.* **158** (2004) 89-105.
[21] A.C.A. Muller, K.L. Scrivener, A.M. Gajewicz and P.J. McDonald, Densification of C-S-H measured by 1H NMR relaxometry, *J. Phys. Chem. C* **117** (2013) 403-412.
[22] Q.H. Do, S. Bishnoi and K. Scrivener, Numerical simulation of porosity in cements, *Transport Porous Med.* (2013).
[23] S.D.C. Walsh, H. Burwinkle and M.O. Saar, A new partial-bounceback lattice-Boltzmann method for fluid flow through heterogeneous media, *Comput. Geosci.* **35** (2009) 1186-1193.
[24] X. He, Q. Zou, L.-S. Luo and M. Dembo, Analytic solutions of simple flows and analysis of nonslip boundary conditions for the lattice Boltzmann BGK model, *J. Stat. Phys.* **87** (1997) 115-136.
[25] A. Narváez and J. Harting, Evaluation of pressure boundary conditions for permeability calculations using the lattice-Boltzmann method, *Adv. Appl. Math. Mech.* **2** (2010) 685-700.
[26] A. Narváez, T. Zauner, F. Raischel, R. Hilfer and J. Harting, Quantitative analysis of numerical estimates for the permeability of porous media from lattice-Boltzmann simulations, *J. Stat. Mech-Theory E.* **11** (2010) P11026.
[27] T.W. Patzek and D.B. Silin, Shape Factor and Hydraulic Conductance in Noncircular Capillaries: I. One-Phase Creeping Flow, *J. Colloid Interf. Sci.* **236** (2001) 295-304.
[28] R.E. Larson and J.J.L. Higdon, A periodic grain consolidation model of porous media, *Phys. Fluids A* **1** (1989) 38-46.
[29] L.J. Parrot and D.C. Killoh, Prediction of cement hydration, *Proc. Br. Ceram. Soc.* **35** (1984) 41-53.
[30] T.C. Powers, Structure and Physical Properties of Hardened Portland Cement Paste, *J. Am. Ceram. Soc.* **41** (1958) 1-6.
[31] A.C.A. Muller, Vacuum saturation of the air voids inside sealed cured cement samples: a nuclear magnetic resonance relaxation analysis, Personal Communication, 2012.
[32] H.S. Wong, M. Zobel, N.R. Buenfeld and R.W. Zimmerman, Influence of the interfacial transition zone and microcracking on the diffusivity, permeability and sorptivity of cement-based materials after drying, *Mag. Concrete Res.* **61** (2009) 571 –589.
[33] W.T. Elam, A.R. Kerstein and J.J. Rehr, Critical Properties of the Void Percolation Problem for Spheres, *Phys. Rev. Lett.* **52** (1984) 1516-1519.